DCPT/08/38
IPPP/08/19

Charged Higgs Bosons in the MSSM at CMS: Discovery Reach and Parameter Dependence

M. Hashemi[1*†], S. Heinemeyer[2‡], R. Kinnunen[3§],
A. Nikitenko[4¶] and G. Weiglein[5‖]

[1] Universiteit Antwerpen, G.U.238, Groenenborgerlaan 171, 2020 Antwerpen, Belgium
[2] Instituto de Fisica de Cantabria (CSIC-UC), Santander, Spain
[3] Helsinki Institute of Physics, Helsinki, Finland
[4] Imperial College, London, UK; on leave from ITEP, Moscow, Russia
[5] IPPP, University of Durham, Durham DH1 3LE, UK

Abstract

The search for MSSM Higgs bosons will be an important goal at the LHC. In order to analyze the search reach of the CMS experiment for the charged MSSM Higgs bosons, we combine the latest results for the CMS experimental sensitivities based on full simulation studies with state-of-the-art theoretical predictions of MSSM Higgs-boson production and decay properties. The experimental analyses are done assuming an integrated luminosity of 30 fb^{-1} for the two cases $M_{H^\pm} < m_t$ and $M_{H^\pm} > m_t$. The results are interpreted as $5\,\sigma$ discovery contours in $M_{H^\pm}$–$\tan\beta$ planes of the MSSM for various benchmark scenarios. We study the dependence of the $5\,\sigma$ contours on the variation of the relevant SUSY parameters. Particular emphasis is put on analyzing the variation of the discovery contours with the Higgs mixing parameter μ. The variation of μ can shift the prospective discovery reach in $\tan\beta$ by up to $\Delta\tan\beta = 40$.

*previously at IPM, Tehran, Iran
† email: Majid.Hashemi@cern.ch
‡ email: Sven.Heinemeyer@cern.ch
§ email: Ritva.Kinnunen@cern.ch
¶ email: Alexandre.Nikitenko@cern.ch
‖ email: Georg.Weiglein@durham.ac.uk

1 Introduction

One of the main goals of the LHC is the identification of the mechanism of electroweak symmetry breaking. The most frequently investigated models are the Higgs mechanism within the Standard Model (SM) and within the Minimal Supersymmetric Standard Model (MSSM) [1]. Contrary to the case of the SM, in the MSSM two Higgs doublets are required. This results in five physical Higgs bosons instead of the single Higgs boson in the SM. These are the light and heavy $\mathcal{CP}$-even Higgs bosons, h and H, the $\mathcal{CP}$-odd Higgs boson, A, and the charged Higgs bosons, $H^\pm$. The Higgs sector of the MSSM can be specified at lowest order in terms of the gauge couplings, the ratio of the two Higgs vacuum expectation values, $\tan\beta \equiv v_2/v_1$, and the mass of the $\mathcal{CP}$-odd Higgs boson, M_A (or $M_{H^\pm}$, the mass of the charged Higgs boson). Consequently, the masses of the $\mathcal{CP}$-even neutral and the charged Higgs bosons are dependent quantities that can be predicted in terms of the Higgs-sector parameters, e.g. $M^2_{H^\pm} = M^2_A + M^2_W$, where M_W denotes the mass of the W boson. The same applies to the production and decay properties of the MSSM Higgs bosons[1]. Higgs-phenomenology in the MSSM is strongly affected by higher-order corrections, in particular from the sector of the third generation quarks and squarks, so that the dependencies on various other MSSM parameters can be important, see e.g. Refs. [2–4] for reviews.

Searches for the charged Higgs bosons of the MSSM (or a more general Two Higgs Doublet Model (THDM)) have been carried out at LEP [5], yielding a bound of $M_{H^\pm} \gtrsim 80$ GeV [6,7]. The Tevatron placed additional bounds on the MSSM parameter space from charged Higgs-boson searches, in particular at large $\tan\beta$ and low M_A [8]. At the LHC the charged Higgs bosons will be accessible best at large $\tan\beta$ up to $M_A \lesssim 800$ GeV [9–11]. At the ILC, for $M_{H^\pm} \lesssim \sqrt{s}/2$ a high-precision determination of the charged Higgs boson properties will be possible [12–15].

The prospective sensitivities at the LHC are usually displayed in terms of the parameters M_A and $\tan\beta$ (or $M_{H^\pm}$ and $\tan\beta$) that characterize the MSSM Higgs sector at lowest order. The other MSSM parameters are conventionally fixed according to certain benchmark scenarios [16]. The respective LHC analyses of the $5\,\sigma$ discovery contours for the charged Higgs boson are given in Ref. [17] for ATLAS and in Refs. [18,19] for CMS. However, within these analyses the variation with relevant SUSY parameters as well as possibly relevant loop corrections in the Higgs production and decay [11] have been neglected.

We focus in this paper on the $5\,\sigma$ discovery contours for the charged MSSM Higgs boson for the two cases $M_{H^\pm} < m_t$ and $M_{H^\pm} > m_t$, within the $m_h^{\rm max}$ scenario and the no-mixing scenario [11,16] (i.e. we concentrate on the $\mathcal{CP}$-conserving case). They are obtained by using the latest CMS results [18,19] derived in a model-independent approach, i.e. making no assumption on the Higgs boson production mechanism or decays. However, the detection relies on the decay mode of the charged Higgs bosons to $\tau\nu_\tau$. Furthermore only SM backgrounds have been assumed. These experimental results are combined with up-to-date theoretical predictions for charged Higgs production and decay in the MSSM, taking into account also the decay to SUSY particles that can in principle suppress the branching ratio of the charged Higgs boson decay to $\tau\nu_\tau$.

For the interpretation of the exclusion bounds and prospective discovery contours in the

[1] If the production or decay involves SUSY particles at tree-level, also other MSSM parameters enter the prediction at lowest order.

benchmark scenarios it is important to assess how sensitively the results depend on those parameters that have been fixed according to the benchmark prescriptions. In Refs. [11, 20] this issue has been analyzed for the neutral heavy MSSM Higgs bosons, and it has been found that the by far largest effect arises from the variation of the Higgs-mixing parameter μ. Consequently, we investigate how the $5\,\sigma$ discovery regions in the $M_{H^\pm}$–$\tan\beta$ plane for the charged MSSM Higgs boson obtainable with the CMS experiment at the LHC are affected by a variation of the mixing parameter μ.

2 Experimental analysis

The main production channels at the LHC are

$$pp \to t\bar{t} \; + \; X, \quad t\bar{t} \to t\, H^- \bar{b} \;\; \text{or} \;\; H^+ b\, \bar{t} \tag{1}$$

and

$$gb \to H^- t \;\; \text{or} \;\; g\bar{b} \to H^+ \bar{t}\; . \tag{2}$$

The decay used in the analysis to detect the charged Higgs boson is

$$H^\pm \;\to\; \tau\nu_\tau \;\to\; \text{hadrons}\; \nu_\tau. \tag{3}$$

The analyses described below correspond to CMS experimental sensitivities based on full simulation studies, assuming an integrated luminosity of 30 fb^{-1}. In these analyses a top quark mass of $m_t = 175$ GeV has been assumed.

2.1 The light charged Higgs Boson

The "light charged Higgs boson" is characterized by $M_{H^\pm} < m_t$. The main production channel is given in eq. (1). Close to threshold also eq. (2) contributes. The relevant (i.e. detectable) decay channel is given by eq. (3). The experimental analysis, based on 30 fb^{-1} collected with CMS, is presented in Ref. [18]. The events were required to be selected with the single lepton trigger, thus exploiting the $W \to \ell\nu$ decay mode of a W boson from the decay of one of the top quarks in eq. (1).

The total number of events leading to final states with the signal characteristics is evaluated, including their respective experimental efficiencies. The various channels and the corresponding efficiencies can be found in Tab. 1. The efficiencies are given for $M_{H^\pm} = 160$ GeV, but vary only insignificantly over the parameter space under investigation. The number of signal-like events is evaluated as the sum of background and Higgs-boson signal events,

$$\begin{aligned} N_{\text{ev}} = {} & N_{\text{background}}(\text{from the processes in Tab. 1}) \\ & + \mathcal{L} \times \sigma(pp \to t\bar{t} + X) \times \text{BR}(t \to H^\pm b) \times \text{BR}(H^\pm \to \tau\nu_\tau) \\ & \qquad \times \text{BR}(\tau \to \text{hadrons}) \times \text{exp. eff.}\; , \end{aligned} \tag{4}$$

where $\mathcal{L}$ denotes the luminosity, and the experimental efficiency is given in Tab. 1. A $5\,\sigma$ discovery can be achieved if a parameter point results in more than 5260 events (with 30 fb^{-1}).

We furthermore used

$$\begin{aligned} \mathrm{BR}(W^\pm \to \ell\nu_\ell) &= 0.217 \;\; (\ell = \mu, e), \\ \mathrm{BR}(W^\pm \to \tau\nu_\tau) &= 0.1085, \\ \mathrm{BR}(W^\pm \to \text{jets}) &= 0.67, \\ \mathrm{BR}(\tau \to \text{hadrons}) &= 0.65. \end{aligned} \tag{5}$$

The next-to-leading order LHC cross section for top quark pairs is taken to be 840 pb [21]. For the $W^\pm$+3 jets background the leading order cross section for the process $pp \to W^\pm + 3$ jets, $W^\pm \to \ell^\pm\nu$ ($\ell = e,\ \mu$) of 840 pb was used, as given by the MadGraph [22] generator.

channel	exp. efficiency
$pp \to t\bar{t} + X,\ t\bar{t} \to H^+ b\,\bar{t} \to (\tau^+\bar{\nu}_\tau)\ b\ (W^-\bar{b});\ \ \tau \to$ hadrons, $W \to \ell\nu_\ell$	0.0052
$pp \to t\bar{t} + X,\ t\bar{t} \to W^+\,W^-\,b\bar{b} \to (\tau\nu_\tau)\ (\ell\nu_\ell)\ b\bar{b};\ \ \tau \to$ hadrons	0.00217
$pp \to t\bar{t} + X,\ t\bar{t} \to W^+\,W^-\,b\bar{b} \to (\ell\nu_\ell)\ (\ell\nu_\ell)\ b\bar{b}$	0.000859
$pp \to t\bar{t} + X,\ t\bar{t} \to W^+\,W^-\,b\bar{b} \to$ (jet jet) $(\ell\nu_\ell)\ b\bar{b}$	0.000134
$pp \to W + 3$ jets, $W \to \ell\nu$	0.000013

Table 1: Relevant signal (first line) and background channels for the light charged Higgs boson and their respective experimental efficiencies. The charge conjugated processes ought to be included. The efficiency for the charged Higgs production is given for $M_{H^\pm} = 160$ GeV, but varies only insignificantly over the relevant parameter space. ℓ denotes e or μ.

2.2 The heavy charged Higgs Boson

The "heavy charged Higgs boson" is characterized by $M_{H^\pm} \gtrsim m_t$. Here eq. (2) gives the largest contribution to the production cross section, and very close to threshold eq. (1) can contribute somewhat. The relevant decay channel is again given in eq. (3). The experimental analysis, based on 30 fb^{-1} collected with CMS, has been presented in Ref. [19]. The fully hadronic final state topology was considered, thus events were selected with the single τ trigger at Level-1 and the combined τ-$E_{\mathrm{T}}^{\mathrm{miss}}$ High Level trigger. The backgrounds considered were $t\bar{t}$, $W^\pm t$, $W^\pm + 3$ jets as well as QCD multi-jet background. The $t\bar{t}$ and QCD multi-jet processes were generated with PYTHIA [23], $W^\pm t$ was generated with the TopRex generator [24] and $W^\pm + 3$ jets with MadGraph [22]. The production cross sections for the $t\bar{t}$ background processes were normalized to the NLO cross sections [21]. The total background amounts (after cuts) to 1.7 ± 1 events, independently of the charged Higgs boson mass.

The number of signal events is evaluated as

$$N_{\mathrm{ev}} = \mathcal{L} \times \sigma(pp \to H^\pm + X) \times \mathrm{BR}(H^\pm \to \tau\nu_\tau) \times \mathrm{BR}(\tau \to \text{hadrons}) \times \text{exp. eff.}\ , \tag{6}$$

where $\mathcal{L}$ denotes the luminosity, and the experimental efficiency is given in Tab. 2 as a function of $M_{H^\pm}$. A $5\,\sigma$ discovery corresponds to a number of signal events larger than 14.1.

$M_{H^\pm}$ [GeV]	171.6	180.4	201.0	300.9	400.7	600.8
exp. eff. [10^{-4}]	3.5	4.0	5.0	23	32	42

Table 2: Experimental efficiencies for the heavy charged Higgs boson detection.

The efficiency for the charged Higgs boson production over the full mass range considered was evaluated with the PYTHIA [23] generator processes 401 ($gg \to tbH^\pm$) and 402 ($qq \to tbH^\pm$) implemented as described in Ref. [25].

3 Calculation of cross section and branching ratios

While the phenomenology of the production and decay processes of the charged MSSM Higgs bosons at the LHC is mainly characterized by the parameters M_A (or $M_{H^\pm}$) and $\tan\beta$ that govern the Higgs sector at lowest order, other MSSM parameters enter via higher-order contributions (see e.g. Ref. [11] and references therein), and also via the kinematics of Higgs-boson decays into supersymmetric particles. The other MSSM parameters are usually fixed in terms of benchmark scenarios. The most commonly used scenarios are the "$m_h^{\rm max}$" and "no-mixing" benchmark scenarios [11, 16]. According to the definition of Ref. [16] the $m_h^{\rm max}$ scenario is given by,

$$\begin{aligned} \underline{m_h^{\rm max}:} \quad & M_{\rm SUSY} = 1000 \text{ GeV}, \quad X_t = 2\, M_{\rm SUSY}, \quad A_b = A_t, \\ & \mu = 200 \text{ GeV}, \quad M_2 = 200 \text{ GeV}, \quad m_{\tilde g} = 0.8\, M_{\rm SUSY} \ . \end{aligned} \tag{7}$$

Here $M_{\rm SUSY}$ denotes the diagonal soft SUSY-breaking parameters in the sfermion mass matrices, $m_t\, X_t \equiv m_t\,(A_t - \mu/\tan\beta)$ is the off-diagonal entry in the scalar top mass matrix. $A_{t(b)}$ denote the trilinear Higgs-stop (-sbottom) couplings, μ is the Higgs mixing parameter, $m_{\tilde g}$ the gluino mass, and M_2 and M_1 denote the soft SUSY-breaking parameters in the chargino/neutralino sector. The parameter M_1 is fixed via the GUT relation $M_1 = (5 s_W^2)/(3 c_W^2)\, M_2$. The no-mixing scenario differs from the $m_h^{\rm max}$ scenario only in the definition of vanishing mixing in the stop sector and a larger value of $M_{\rm SUSY}$,

$$\begin{aligned} \underline{\text{no-mixing:}} \quad & M_{\rm SUSY} = 2000 \text{ GeV}, \quad X_t = 0, \quad A_b = A_t, \\ & \mu = 200 \text{ GeV}, \quad M_2 = 200 \text{ GeV}, \quad m_{\tilde g} = 0.8\, M_{\rm SUSY} \ . \end{aligned} \tag{8}$$

The value of the top-quark mass in Ref. [16] was chosen according to the experimental central value at that time. For our numerical analysis below, we use the value, $m_t = 175$ GeV, see Sect. 2. Using the current value of $m_t = 172.6$ GeV [26] would lead to a small shift of the discovery contours right at threshold, but is insignificant for the qualitative results of this analysis.

In Ref. [11] it was suggested that in the search for heavy MSSM Higgs bosons the $m_h^{\rm max}$ and no-mixing scenarios, which originally were mainly designed for the search for the light $\mathcal{CP}$-even Higgs boson h, should be extended by several discrete values of μ (see below),

$$\mu = \pm 200, \pm 500, \pm 1000 \text{ GeV} \ . \tag{9}$$

In our analyses here we focus on $\mu = \pm 200, \pm 1000$ GeV.

For the calculation of cross sections and branching ratios we use a combination of up-to-date theory evaluations. The interaction of the charged Higgs boson with the t/b doublet can be expressed in terms of an effective Lagrangian [27],

$$\mathcal{L} = \frac{g}{2M_W} \frac{\overline{m}_b}{1+\Delta_b} \left[\sqrt{2}\, V_{tb}\, \tan\beta\, H^+ \bar{t}_L b_R \right] + \text{h.c.} \tag{10}$$

Here $\overline{m}_b$ denotes the running bottom quark mass including SM QCD corrections. The prefactor $1/(1+\Delta_b)$ in eq. (10) arises from the resummation of the leading $\tan\beta$-enhanced corrections to all orders. The explicit form of Δ_b in the limit of heavy SUSY masses and $\tan\beta \gg 1$ reads [28]

$$\Delta_b = \frac{2\alpha_s}{3\,\pi}\, m_{\tilde{g}}\, \mu\, \tan\beta\, \times\, I(m_{\tilde{b}_1}, m_{\tilde{b}_2}, m_{\tilde{g}}) + \frac{\alpha_t}{4\,\pi}\, A_t\, \mu\, \tan\beta\, \times\, I(m_{\tilde{t}_1}, m_{\tilde{t}_2}, |\mu|)\ . \tag{11}$$

Here $m_{\tilde{t}_1}$, $m_{\tilde{t}_2}$, $m_{\tilde{b}_1}$, $m_{\tilde{b}_2}$ denote the $\tilde{t}$ and $\tilde{b}$ masses. α_s is the strong coupling constant, while $\alpha_t \equiv h_t^2/(4\pi)$ is defined via the top Yukawa coupling. The analytical expression for $I(\ldots)$ can be found in Ref. [11]. Large negative values of $(\mu\, m_{\tilde{g}})$ and $(\mu\, A_t)$ (it should be noted that both benchmark scenarios have positive $m_{\tilde{g}}$ and A_t) can lead to a strong enhancement of the $H^\pm tb$ coupling, while large positive values lead to a strong suppression. Concerning the $m_h^{\rm max}$ and the no-mixing benchmark scenarios, as discussed in Refs. [11, 20] the Δ_b effects are much more pronounced in the $m_h^{\rm max}$ scenario, where the two terms in eq. (11) are of similar size. In the no-mixing scenario the first term in eq. (11) dominates, while the second term is small. A further suppression is caused by the larger value of $M_{\rm SUSY}$ (see eq. (8)) in comparison with the $m_h^{\rm max}$ scenario. Consequently, the total effect of Δ_b is smaller in the no-mixing scenario (see also the discussion in Ref. [11]).

For the production cross section in eq. (1) we use the SM cross section $\sigma(pp \to t\bar{t}) = 840$ pb [21][2] times the BR($t \to H^\pm\, b$) including the Δ_b corrections described above. The production cross section in eq. (2) is evaluated as given in Refs. [30, 31]. In addition also the Δ_b corrections of eq. (10) are applied. Finally the BR($H^\pm \to \tau\nu_\tau$) is evaluated taking into account all decay channels, among which the most relevant are $H^\pm \to tb, cs, W^{(*)}h$. Also possible decays to SUSY particles are taken into account. For the decay to tb again the Δ_b corrections are included. All the numerical evaluations are performed with the program `FeynHiggs` [32–35], see also Ref. [36].

4 Numerical analysis

The numerical analysis has been performed in the $m_h^{\rm max}$ and the no-mixing scenarios [11, 16] for $\mu = -1000, -200, +200, +1000$ GeV. We separately present the results for the light and the heavy charged Higgs and finally compare with the results in the CMS PTDR, where the results had been obtained fixing $\mu = +200$ GeV and neglecting the Δ_b corrections, as well as neglecting the charged Higgs-boson decays to SUSY particles.

[2] The corresponding SUSY corrections are small [29] and have been neglected.

4.1 The light charged Higgs boson

In Fig. 1 we show the results for the $5\,\sigma$ discovery contours for the light charged Higgs boson, corresponding to the experimental analysis in Sect. 2.1, where the charged Higgs boson discovery will be possible in the areas above the curves shown in Fig. 1. As described above, the experimental analysis was performed for the CMS detector and 30 fb^{-1}. The top quark mass is set to $m_t = 175$ GeV. The thick (thin) lines correspond to positive (negative) μ, and the solid (dotted) lines have $|\mu| = 1000(200)$ GeV. The curves stop at $\tan\beta = 60$, where we stopped the evaluation of production cross section and branching ratios. For negative μ very large values of $\tan\beta$ result in a strong enhancement of the bottom Yukawa coupling, and for $\Delta_b \to -1$ the MSSM enters a non-perturbative regime, see eq. (10).

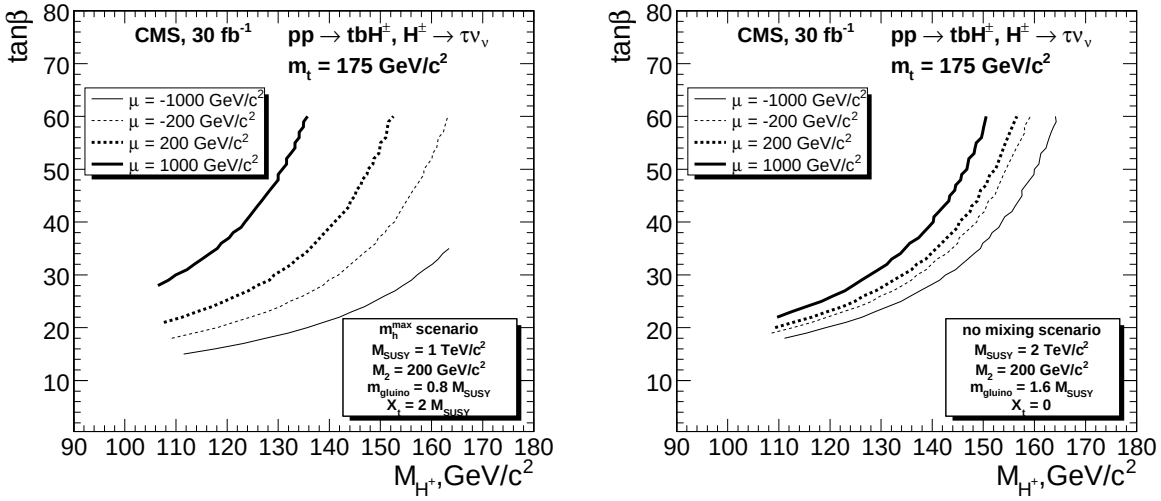

Figure 1: Discovery reach for the light charged Higgs boson of CMS with 30 fb^{-1} in the $M_{H^\pm}$–$\tan\beta$ plane for the $m_h^{\max}$ scenario (left) and the no-mixing scenario (right).

Within the $m_h^{\max}$ scenario, shown in the left plot of Fig. 1, the search for the light charged Higgs boson covers the area of large $\tan\beta$ and $M_{H^\pm} \lesssim 130 \ldots 160$ GeV. The variation with μ induces a strong shift in the $5\,\sigma$ discovery contours. This corresponds to a shift in $\tan\beta$ of $\Delta\tan\beta = 15$ for $M_{H^\pm} \lesssim 110$ GeV, rising up to $\Delta\tan\beta = 40$ for larger $M_{H^\pm}$ values. The discovery region is largest (smallest) for $\mu = -(+)1000$ GeV, corresponding to the largest (smallest) production cross section. The results for the no-mixing scenario are shown in the right plot of Fig. 1. The effects of the variation of μ are much less pronounced in this scenario, as discussed in Sect. 3, due to the smaller absolute value of Δ_b (see also the corresponding analysis for neutral heavy Higgs bosons in Ref. [20]). The shift in $\tan\beta$ for $M_{H^\pm} = 110$ GeV is about $\Delta\tan\beta = 5$ going from $\mu = -1000$ GeV to $+1000$ GeV. For $\tan\beta = 60$ (where we stop our analysis) the covered $M_{H^\pm}$ values range from 150 GeV to 164 GeV. In this charged Higgs boson mass range for the considered benchmark scenarios no decay channels into SUSY particles are open, i.e. the observed effects are all due to higher-order corrections, in particular associated with Δ_b.

4.2 The heavy charged Higgs boson

In Fig. 2 we show the results for the $5\,\sigma$ discovery contours for the heavy charged Higgs boson, corresponding to the experimental analysis in Sect. 2.2. The Higgs boson discovery will be possible in the areas above the curves.[3] As before, the experimental analysis was performed for the CMS detector and 30 fb^{-1}. The top quark mass is set to $m_t = 175$ GeV. The thick (thin) lines correspond to positive (negative) μ, and the solid (dotted) lines have $|\mu| = 1000(200)$ GeV.

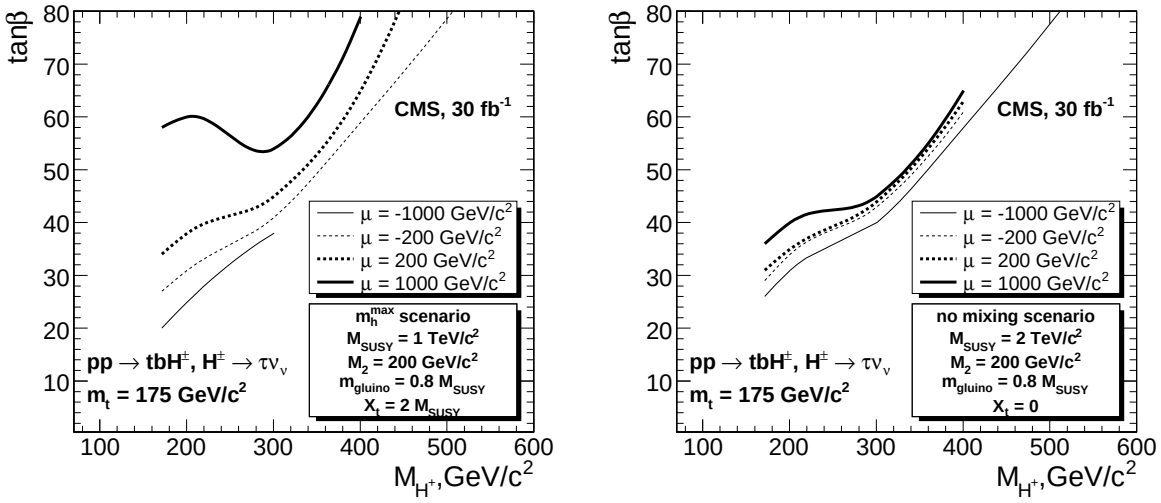

Figure 2: Discovery reach for the heavy charged Higgs boson of CMS with 30 fb^{-1} in the $M_{H^\pm}$–$\tan\beta$ plane for the $m_h^{\max}$ scenario (left) and the no-mixing scenario (right).

The $5\,\sigma$ discovery regions for the search for heavy charged Higgs bosons in the $m_h^{\max}$ scenario are shown in the left plot of Fig. 2. For $M_{H^\pm} = 170$ GeV, where the experimental analysis stops, we find a strong variation in the accessible parameter space for $\mu = -(+)1000$ GeV of $\Delta \tan\beta = 40$. It should be noted in this context that close to threshold, where both production mechanisms, eqs. (1) and (2), contribute, the theoretical uncertainties are somewhat larger than in the other regions. For $M_{H^\pm} = 300$ GeV the variation in the $5\,\sigma$ discovery contours goes from $\tan\beta = 38$ to $\tan\beta = 54$. For $\mu = -1000$ GeV and larger $\tan\beta$ values the bottom Yukawa coupling becomes so large that a perturbative treatment would no longer be reliable in this region, and correspondingly we do not continue the respective curve(s).

The shape of the $\mu = +1000$ GeV curve has a local minimum at $M_{H^\pm} \approx 300$ GeV that is not (or only very weakly) present in the other curves, and that is also not visible in the original CMS analysis in Ref. [19] (obtained for $\mu = +200$ GeV, but neglecting the Δ_b effects). The reason for the local minimum can be traced back to the strongly improved experimental efficiency going from $M_{H^\pm} = 200$ GeV to 300 GeV, see Tab. 2. The better efficiency at $M_{H^\pm} = 300$ GeV corresponds to a lower required cross section ($\propto \tan^2\beta$) and/or a lower BR($H^\pm \to \tau\nu_\tau$) to obtain the same number of signal events. On the other

[3] An analysis in other benchmark scenarios that are in agreement with the cold dark matter density constraint imposed by WMAP and other cosmological data [37] can be found in Ref. [38].

hand, going from $M_{H^\pm} = 200$ GeV to 300 GeV this effect is in most cases overcompensated by a decrease of the cross section due to the increase in $M_{H^\pm}$. The overcompensation results in an increase in $\tan\beta$ for the higher $M_{H^\pm}$ value. For $\mu = +1000$ GeV, however, Δ_b is very large, suppressing strongly the charged Higgs production cross section as well as the $\mathrm{BR}(H^\pm \to tb)$. The overall effect is a somewhat better reach in $\tan\beta$ for $M_{H^\pm} = 300$ GeV than for $M_{H^\pm} = 200$ GeV.

In comparison with the analysis of Ref. [11], based on the older CMS analysis given in Ref. [39], several differences can be observed. The feature of the local minimum is absent in Ref. [11], the variation of the $5\,\sigma$ discovery contours with μ is weaker, and the effect of the decay of the charged Higgs boson to a chargino and a neutralino is more pronounced in Ref. [11]. The reason for these differences is the strongly reduced discovery region in the new CMS analysis [19] employed here as compared to the old CMS analysis [39] used in Ref. [11]. The reach in $\tan\beta$ is worse by $\sim 15(30)$ for $M_A = 200(400)$ GeV in the new analysis.[4] Thus, at the substantially worse (i.e. higher) $\tan\beta$ values employed here the Δ_b effects are more pronounced, leading to the local minimum for $\mu = +1000$ GeV and to a larger absolute variation in $\tan\beta$ with the size and the sign of μ, see Sect. 3. In the high $\tan\beta$ region furthermore the Δ_b effects dominate over the impact of the decay of the charged Higgs to charginos and neutralinos. As an example, for $\mu = +200$ GeV and $M_{H^\pm} = 400$ GeV the old analysis in Ref. [11] found that the discovery region starts at $\tan\beta = 32$, where $\mathrm{BR}(H^\pm \to \tilde{\chi}^\pm\tilde{\chi}^0) \approx 15\%$. Here we find that the discovery region starts at $\tan\beta = 64$, where $\mathrm{BR}(H^\pm \to \tilde{\chi}^\pm\tilde{\chi}^0) \approx 3\%$.

The no-mixing scenario is shown in the right plot of Fig. 2. The features are the same as in the m_h^{max} scenario. However, due to the smaller size of $|\Delta_b|$, see Sect. 3, they are much less pronounced. The variation in $\tan\beta$ stays at or below the level of $\Delta\tan\beta = 10$ for the whole range of $M_{H^\pm}$.

4.3 Comparison with the CMS PTDR

In Fig. 3 we show the combined results for the $5\,\sigma$ discovery contours for the light and the heavy charged Higgs boson, corresponding to the experimental analyses in the m_h^{max} scenario as presented in the two previous subsections. They are compared with the results presented in the CMS PTDR [10]. Contrary to the previous sections, we now show the $5\,\sigma$ discovery contours in the M_A–$\tan\beta$ plane. The thick (thin) lines correspond to positive (negative) μ, and the solid (dotted) lines have $|\mu| = 1000(200)$ GeV. The thickened dotted (red/blue) lines represent the CMS PTDR results, obtained for $\mu = +200$ GeV and neglecting the Δ_b effects.

Apart from the variation in the $5\,\sigma$ discovery contours with the size and the sign of $|\mu|$, two differences can be observed in the comparison of the PTDR results to the new results obtained here, i.e. including the Δ_b corrections in the production and decay of the charged Higgs boson as well as taking the decay to SUSY particles into account. For the light charged Higgs analysis the discovery contours are now shifted to smaller M_A values, for negative μ even "bending over" for larger $\tan\beta$ values. The reason is the more complete inclusion of higher-order corrections (full one-loop and leading $\mathcal{O}(\alpha_t\alpha_s)$ two-loop) to the relation between

[4] The old analysis uses $\mu = -200$ GeV [39], while the new analysis set $\mu = +200$ GeV [19]. However, since the Δ_b corrections are neglected in Refs. [19, 39], the effect on the discovery regions should be small.

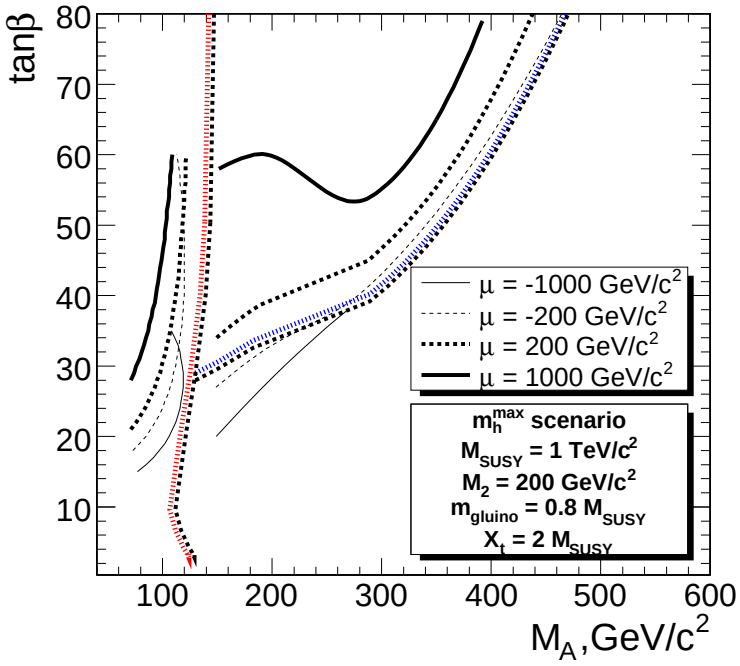

Figure 3: Discovery reach for the charged Higgs boson of CMS with 30 fb^{-1} in the M_A–$\tan\beta$ plane for the $m_h^{\max}$ scenario for $\mu = \pm 200, \pm 1000$ GeV in comparison with the results from the CMS PTDR (thickened dotted (red and blue) lines), obtained for $\mu = +200$ GeV and neglecting the Δ_b effects.

M_A and $M_{H^\pm}$ [35, 36]. The second feature is a small gap between the light and the heavy charged Higgs analyses, while in the PTDR analysis all charged Higgs masses could be accessed. The gap can be observed best by comparing the $m_h^{\max}$ scenario in Figs. 1 and 2. This gap is largest for $\mu = +1000$ GeV and smallest for $\mu = -1000$ GeV, where it amounts only up to ~ 5 GeV. Possibly the heavy charged Higgs analysis strategy exploiting the fully hadronic final state can be extended to smaller M_A values to completely close the gap. For the interpretation of Fig. 3 it should be kept in mind that the accessible area in the heavy Higgs analysis also "bends over" to smaller M_A values for larger $\tan\beta$, thus decreasing the visible gap in Fig. 3.

5 Conclusions

We have studied the variation of the $5\,\sigma$ discovery contours for the search for the charged MSSM Higgs boson with the SUSY parameters. We combine the latest results for the CMS experimental sensitivities based on full simulation studies with state-of-the-art theoretical predictions of MSSM Higgs-boson properties. The experimental analyses are done assuming an integrated luminosity of 30 fb^{-1} for the two cases, $M_{H^\pm} < m_t$ and $M_{H^\pm} > m_t$.

The numerical analysis has been performed in the $m_h^{\max}$ and the no-mixing scenarios for $\mu = \pm 200, \pm 1000$ GeV. The impact of the variation of μ enters in particular via the higher-

order correction Δ_b, affecting the charged Higgs production cross section and branching ratios. Also the decays of the charged Higgs boson to SUSY particles have been taken into account. As a general feature, large negative μ values give the largest reach, while large positive values yield the smallest $5\,\sigma$ discovery areas.

The search for the light charged Higgs boson covers the the area of large $\tan\beta$ and $M_{H^\pm} \lesssim 160$ GeV. The variation with μ within the $m_h^{\rm max}$ scenario induces a strong shift in the $5\,\sigma$ discovery contours with $\Delta\tan\beta = 15$ for $M_{H^\pm} = 100$ GeV, rising up to $\Delta\tan\beta = 40$ for larger $M_{H^\pm}$ values. The discovery region is largest (smallest) for $\mu = -(+)1000$ GeV, corresponding to the largest (smallest) production cross section. The effects are similar, but much less pronounced, in the no-mixing scenario.

The search for the heavy charged Higgs boson reaches up to $M_{H^\pm} \lesssim 400$ GeV for large $\tan\beta$. Within the $m_h^{\rm max}$ scenario the variation of μ induces a very strong shift in the $5\,\sigma$ discovery contours of up to $\Delta\tan\beta = 40$ for $M_{H^\pm} \gtrsim m_t$. As in the light charged Higgs case, within the no-mixing scenario the effects show the same qualitative behavior, but are much less pronounced.

Combining the search for the light and the heavy charge Higgs boson, we find a small gap, while in the CMS Physics Technical Design Report analysis all charged Higgs masses could be accessed. Possibly the heavy charged Higgs analysis strategy exploiting the fully hadronic final state can be extended to smaller M_A values to completely close the gap. This issue deserves further studies.

Acknowledgements

The work of S.H. was partially supported by CICYT (grant FPA 2007–66387). Work supported in part by the European Community's Marie-Curie Research Training Network under contract MRTN-CT-2006-035505 'Tools and Precision Calculations for Physics Discoveries at Colliders'.

References

[1] H. Nilles, *Phys. Rept.* **110** (1984) 1;
H. Haber and G. Kane, *Phys. Rept.* **117** (1985) 75;
R. Barbieri, *Riv. Nuovo Cim.* **11** (1988) 1.

[2] S. Heinemeyer, W. Hollik and G. Weiglein, *Phys. Rept.* **425** (2006) 265 [arXiv:hep-ph/0412214].

[3] S. Heinemeyer, *Int. J. Mod. Phys.* **A 21** (2006) 2659 [arXiv:hep-ph/0407244].

[4] A. Djouadi, arXiv:hep-ph/0503173.

[5] [LEP Higgs working group], arXiv:hep-ex/0107031.

[6] P. Lutz [LEP Higgs working group], to appear in the proceedings of the LCWS/ILC 2007 workshop, DESY, Hamburg, Germany, May/June 2007.

[7] [LEP Higgs working group], *in preparation*.

[8] [CDF Collaboration], *Phys. Rev. Lett.* **96** (2006) 042003 [arXiv:hep-ex/0510065];
R. Eusebi, PhD thesis: "Search for charged Higgs in $t\bar{t}$ decay products from proton-antiproton collisions at $\sqrt{s} = 1.96\,\mathrm{TeV}$", University of Rochester, 2005.

[9] ATLAS Collaboration, *Detector and Physics Performance Technical Design Report*, CERN/LHCC/99-15 (1999), see:
`atlasinfo.cern.ch/Atlas/GROUPS/PHYSICS/TDR/access.html` .

[10] CMS Collaboration, *Physics Technical Design Report, Volume 2. CERN/LHCC 2006-021*, see: `cmsdoc.cern.ch/cms/cpt/tdr/` .

[11] M. Carena, S. Heinemeyer, C. Wagner and G. Weiglein, *Eur. Phys. J.* **C 45** (2006) 797 [arXiv:hep-ph/0511023].

[12] J. Aguilar-Saavedra et al., TESLA TDR Part 3: "Physics at an e^+e^- Linear Collider", arXiv:hep-ph/0106315, see: `tesla.desy.de/tdr/`;
K. Ackermann et al., DESY-PROC-2004-01, *prepared for 4th ECFA / DESY Workshop on Physics and Detectors for a 90-GeV to 800-GeV Linear e+ e- Collider, Amsterdam, The Netherlands, 1-4 Apr 2003*.

[13] T. Abe et al. [American Linear Collider Working Group Collaboration], arXiv:hep-ex/0106056.

[14] K. Abe et al. [ACFA Linear Collider Working Group Collaboration], arXiv:hep-ph/0109166.

[15] S. Heinemeyer et al., arXiv:hep-ph/0511332.

[16] M. Carena, S. Heinemeyer, C. Wagner and G. Weiglein, *Eur. Phys. J.* **C 26** (2003) 601 [arXiv:hep-ph/0202167].

[17] K. Assamagan, Y. Coadou and A. Deandrea, *Eur. Phys. J. direct* **C 4** (2002) 9 [arXiv:hep-ph/0203121];
K. Assamagan and N. Gollub, *Eur. Phys. J.* **C 39S2** (2005) 25 [arXiv:hep-ph/0406013].

[18] M. Baarmand, M. Hashemi and A. Nikitenko, CMS Note 2006/056.

[19] R. Kinnunen, CMS Note 2006/100.

[20] S. Gennai, S. Heinemeyer, A. Kalinowski, R. Kinnunen, S. Lehti, A. Nikitenko and G. Weiglein, *Eur. Phys. J.* **C 52** (2007) 383 [arXiv:0704.0619 [hep-ph]].

[21] P. Nason, S. Dawson and R. K. Ellis, *Nucl. Phys.* **B 303** (1988) 607;
W. Beenakker, H. Kuijf, W. van Neerven and J. Smith, *Phys. Rev.* **D 40** (1989) 54;
for more details see:
M. Beneke et al., arXiv:hep-ph/0003033, and references therein.

[22] W. Long and T. Stelzer, *Comput. Phys. Commun.* **81** (1994) 357 [arXiv:hep-ph/9401258];
F. Maltoni and T. Stelzer, *JHEP* **0302** (2003) 027 [arXiv:hep-ph/0208156].

[23] T. Sjostrand et al., *Comput. Phys. Commun.* **135** (2001) 238 [arXiv:hep-ph/0010017].

[24] S. Slabospitsky and L. Sonnenschein, *Comput. Phys. Commun.* **148** (2002) 87 [arXiv:hep-ph/0201292].

[25] J. Alwall and J. Rathsman, *JHEP* **0412** (2004) 050 [arXiv:hep-ph/0409094].

[26] Tevatron Electroweak Working Group, axXiv:0803.1683 [hep-ex];
see: `tevewwg.fnal.gov/top/` .

[27] M. Carena, D. Garcia, U. Nierste and C. Wagner, *Nucl. Phys.* **B 577** (2000) 577 [arXiv:hep-ph/9912516].

[28] R. Hempfling, *Phys. Rev.* **D 49** (1994) 6168;
L. Hall, R. Rattazzi and U. Sarid, *Phys. Rev.* **D 50** (1994) 7048 [arXiv:hep-ph/9306309];
M. Carena, M. Olechowski, S. Pokorski and C. Wagner, *Nucl. Phys.* **B 426** (1994) 269 [arXiv:hep-ph/9402253].

[29] W. Beenakker, A. Denner, W. Hollik, R. Mertig, T. Sack and D. Wackeroth, *Nucl. Phys.* **B 411** (1994) 343;
H. Zhou and C. Li, *Phys. Rev.* **D 55** (1997) 4421;
W. Hollik, W. Mösle and D. Wackeroth, *Nucl. Phys.* **B 516** (1998) 29 [arXiv:hep-ph/9706218].

[30] T. Plehn, *Phys. Rev.* **D 67** (2003) 014018 [arXiv:hep-ph/0206121].

[31] E. Berger, T. Han, J. Jiang and T. Plehn, *Phys. Rev.* **D 71** (2005) 115012 [arXiv:hep-ph/0312286].

[32] S. Heinemeyer, W. Hollik and G. Weiglein, *Comput. Phys. Commun.* **124** (2000) 76, [arXiv:hep-ph/9812320]; see: `www.feynhiggs.de` .

[33] S. Heinemeyer, W. Hollik and G. Weiglein, *Eur. Phys. J.* **C 9** (1999) 343 [arXiv:hep-ph/9812472].

[34] G. Degrassi, S. Heinemeyer, W. Hollik, P. Slavich and G. Weiglein, *Eur. Phys. J.* **C 28** (2003) 133 [arXiv:hep-ph/0212020].

[35] M. Frank, T. Hahn, S. Heinemeyer, W. Hollik, H. Rzehak and G. Weiglein, *JHEP* **0702** (2007) 047 [arXiv:hep-ph/0611326].

[36] S. Heinemeyer, W. Hollik, H. Rzehak and G. Weiglein, *Phys. Lett.* **B 652** (2007) 300 [arXiv:0705.0746 [hep-ph]].

[37] C. Bennett et al., *Astrophys. J. Suppl.* **148** (2003) 1 [arXiv:astro-ph/0302207];
D. Spergel et al. [WMAP Collaboration], *Astrophys. J. Suppl.* **148** (2003) 175 [arXiv:astro-ph/0302209];
D. Spergel et al. [WMAP Collaboration], *Astrophys. J. Suppl.* **170** (2007) 377 [arXiv:astro-ph/0603449].

[38] J. Ellis, T. Hahn, S. Heinemeyer, K. Olive and G. Weiglein, *JHEP* **0710** (2007) 092 [arXiv:0709.0098 [hep-ph]].

[39] R. Kinnunen, CMS Note 2005/045.